



Cite this: *Lab Chip*, 2019, 19, 50

## Resolving protein mixtures using microfluidic diffusional sizing combined with synchrotron radiation circular dichroism†

Christian Bortolini, <sup>ab</sup> Tadas Kartanas,<sup>a</sup> Davor Copic,<sup>c</sup> Itzel Condado Morales, <sup>a</sup> Yuewen Zhang, <sup>a</sup> Pavan K. Challa,<sup>a</sup> Quentin Peter, <sup>a</sup> Tamás Jávorfí, <sup>d</sup> Rohanah Hussain, <sup>d</sup> Mingdong Dong, <sup>b</sup> Giuliano Siligardi, <sup>\*d</sup> Tuomas P. J. Knowles <sup>\*ae</sup> and Jérôme Charmet <sup>\*f</sup>

Circular dichroism spectroscopy has become a powerful tool to characterise proteins and other biomolecules. For heterogeneous samples such as those present for interacting proteins, typically only average spectroscopic features can be resolved. Here we overcome this limitation by using free-flow microfluidic size separation in-line with synchrotron radiation circular dichroism to resolve the secondary structure of each component of a model protein mixture containing monomers and fibrils. To enable this objective, we have integrated far-UV compatible measurement chambers into PDMS-based microfluidic devices. Two architectures are proposed so as to accommodate for a wide range of concentrations. The approach, which can be used in combination with other bulk measurement techniques, paves the way to the study of complex mixtures such as the ones associated with protein misfolding and aggregation diseases including Alzheimer's and Parkinson's diseases.

Received 22nd July 2018,  
Accepted 13th November 2018

DOI: 10.1039/c8lc00757h

rsc.li/loc

## 1 Introduction

A range of biophysical tools are available to study homogeneous biomolecule mixtures at the molecular level, but it remains extremely challenging to study heterogeneous mixtures. A particularly striking example is that of proteins associated with misfolding and aggregation diseases, including Alzheimer's and Parkinson's diseases, that aggregate into molecular species of different sizes and solubilities from the very early stages of the disease.<sup>1</sup> Despite significant progress made in recent years, the misfolding pathway remains difficult to fully characterise due in large part to a lack of biophysical tools and methods to study, in molecular detail, such mixtures in their native environment without losing the tem-

poral information of the various molecular changes and interactions.

Bulk measurement techniques such as circular dichroism (CD),<sup>2,3</sup> infrared (IR) spectroscopy,<sup>4,5</sup> nuclear magnetic resonance (NMR)<sup>6,7</sup> or thioflavin T (ThT) fluorescence<sup>8–11</sup> have been used to study protein folding and aggregation. However, such techniques only report on the ensemble average and therefore do not allow for a precise resolution of interactions and changes at the molecular level.

Single molecule techniques, such as atomic force microscopy (AFM),<sup>12,13</sup> electron microscopy (EM),<sup>14,15</sup> infrared nanospectroscopy<sup>16</sup> and high resolution imaging<sup>17,18</sup> have received a considerable interest in recent years to study protein folding and aggregates at the molecular level. For example AFM and transmission electron microscopy (TEM) are commonly used to study peptide self-assembly through the mapping of sample morphology at different aggregation stages.<sup>19–21</sup> To date, however, the level of structural information available from such approaches has been more limited than from bulk spectroscopy. Besides, such measurement often require operation in non-native environment.

Even though conventional separation techniques, such as liquid chromatography, have been combined with bulk measurement techniques to resolve complex mixtures<sup>22–26</sup> their operation usually results in a loss of the temporal information and native environment. For example, it has been acknowledged that the interaction with the stationary phase

<sup>a</sup> Chemistry Department, University of Cambridge, Lensfield Road, Cambridge, CB3 0FF, UK

<sup>b</sup> Interdisciplinary Nanoscience Center, Aarhus University, Aarhus, 8000, Denmark

<sup>c</sup> Institute for Manufacturing, Engineering Department, University of Cambridge, Charles Babbage Road, Cambridge, CB3 0FS, UK

<sup>d</sup> Diamond Light Source, Harwell Science and Innovation Campus, Didcot, OX11 0DE, UK. E-mail: giuliano.siligardi@diamond.ac.uk

<sup>e</sup> Cavendish Laboratory, University of Cambridge, J. J. Thomson Avenue, Cambridge, CB3 0HE, UK. E-mail: tjk2@cam.ac.uk

<sup>f</sup> Institute of Digital Healthcare, WMG, University of Warwick, Coventry, CV4 7AL, UK. E-mail: j.charmet@warwick.ac.uk

† Electronic supplementary information (ESI) available. See DOI: 10.1039/c8lc00757h

and the dilution of the samples in size exclusion chromatography may modify the state of the sample.<sup>27,28</sup>

In recent years, microfluidic approaches have opened up new opportunities to study complex biological processes.<sup>29–32</sup> Here, we take advantage of the laminar flow properties inherent to operation in microfluidic devices to separate a complex mixture into well-resolved size-dependent fractions, using an H-filter configuration.<sup>33</sup> In brief, we flow the solution of interest containing the protein mixture, alongside a buffer solution. The different components of the mixture diffuse in a size-dependent manner, into the buffer solution and the free-flowing solution is then separated into well resolved fractions (see Fig. 1). The concentration of the isolated fraction is obtained based on the concentration profile (Fig. 1c) calculated by numerically solving the problem of particles diffusing in a fully developed Poiseuille flow in a rectangular microfluidics channel (see Calculation of the diffusion profile section). The fractions are then studied with a label-free bulk measurement technique, in this case synchrotron radiation circular dichroism (SRCD), a powerful technique to study the secondary structure of chiral molecules (see Synchrotron radiation circular dichroism section). In particular, we use the highly collimated microbeam generated at Diamond B23 beamline for SRCD,<sup>34</sup> which enables on-chip measurement. We show that this combination gives information that could not be obtained by studying the complex mixture without

separation. In particular, we demonstrate that by excluding larger species from one fraction (fraction 2 in Fig. 1), it is possible to resolve precisely its structure and reconstruct the structure of the other species (fraction 2) by subtracting the spectrum of the resolved fraction from the that of the overall mixture. Even though the concept proposed herein is used with SRCD, it is can also be adapted to other bulk measurement techniques, such as UV/vis, IR absorption and fluorescence microscopy.

A challenge encountered in interfacing microfluidics with CD is the incompatibility of conventional polydimethylsiloxane (PDMS) based microfluidic devices with Dd-UV measurement (see Fig. S1†). Even though the combination of SRCD and microfluidics has been reported previously to study protein refolding kinetics of cytochrome C from 4 M to 0.8 M GuHCl,<sup>35</sup> the mixing devices used in these studies were made of fused silica with the beamlight focused on a masked slit of 60  $\mu\text{m} \times 15$  mm. The fabrication of such devices requires access to specialised microfabrication equipment and expertise, which is usually not readily available in conventional biophysical laboratories. Since soft-lithography is one of the most widely used technique to fabricate microfluidic devices,<sup>36,37</sup> and in an effort to make our finding available to a broad scientific community, we propose here microfluidic devices fabricated using conventional PDMS-based soft-lithography, compatible with far-UV measurement, including

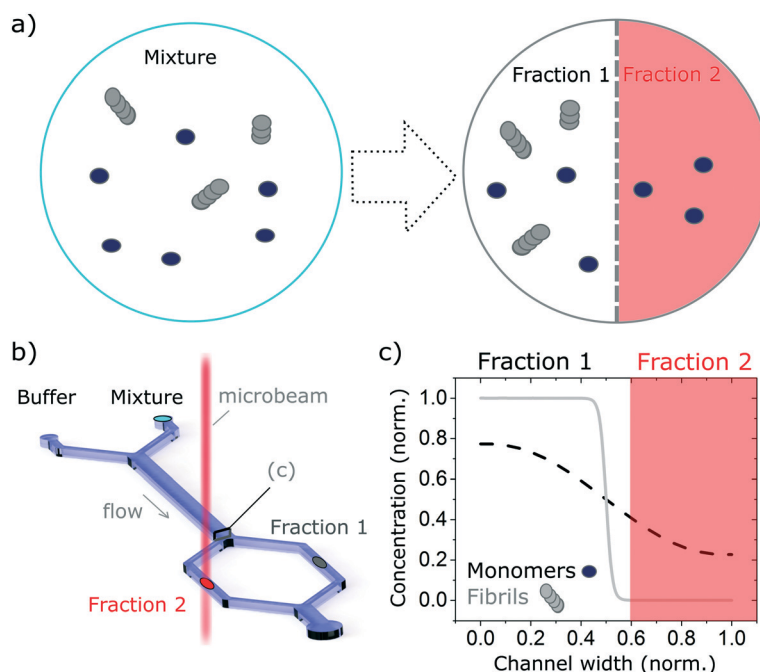


**Fig. 1** Schematic of the measurement principle. The combination of microfluidics-based free-flow separation with bulk measurement technique enables the study, in molecular detail, of heterogeneous mixtures in their native environment while retaining the temporal information. In this manuscript we combine diffusion-based separation with the ability to measure SRCD using the highly collimated microbeam of B23 beamline to study proteins mixtures. (a) The complex mixture, here made up of monomers and fibrils, is flown alongside a buffer solution. The monomers, with a smaller hydrodynamic radius, diffuse faster than the fibres, enabling the separation of the mixture into well-defined fractions that can be studied separately. (b) Sketch of the diffusion-based separation microfluidic device and microbeam light to probe each fraction. (c) Diffusion profile of the monomers and fibrils normalised concentrations at the end of the microfluidics device diffusion length. The fractions collected depend on the hydrodynamic resistance of the separation channels (normalised channel width).

SRCD. In this manuscript, we describe proof-of-principle microfluidic devices based on two architectures enabling the integration of measurement chambers of different height, thus allowing the measurement of a wide range of concentration (see Fig. 2).

## 2 Materials and methods

### Sample preparation

Insulin fibrils were assembled *in vitro* by incubating 348  $\mu\text{M}$  (2 mg  $\text{mL}^{-1}$ ) of bovine insulin (Sigma Aldrich) in HCl (pH 1.4) for 8 hours at 60 °C on non-binding plates (half-volume, CORNING 3881). The fibril formation was evaluated using controls insulin were incubated under the same conditions with ThT (40  $\mu\text{M}$ ) as shown in Fig. S2† The unlabelled fibrils were then sonicated to homogenise the mixture into approximately 100 nm long fibres (Fig. S3† for TEM images) and diluted in water to the desired concentration. Insulin and BSA monomers (Sigma Aldrich) were dissolved in HCl (pH 1.4) and phosphate buffer (pH 2.7) respectively and directly diluted to the desired concentration in water.

### Synchrotron radiation circular dichroism

Circular dichroism (CD), a spectroscopic technique used to probe conformational changes of chiral molecules<sup>2,3–38</sup> is particularly well suited to study protein folding and aggregation. In the case of proteins, CD is mainly employed to assess their secondary structure and conformation by measuring the ab-

sorption of circularly polarised light in the protein backbone. If the contribution to the CD signal of the side chains is neglected, which is usually a good approximation, information about protein folding can be accurately estimated, even when analysing samples at very low concentration and with composite  $\alpha$ -helical and  $\beta$ -sheet domains.<sup>2</sup> The far-UV region of CD spectra (from 180 to 240 nm) exhibits typical absorption characteristics of  $\alpha$ -helices (190 and 208 nm for  $\pi \rightarrow \pi^*$ , 222 nm for  $n \rightarrow \pi^*$ ) and  $\beta$ -sheets (195 nm for  $\pi \rightarrow \pi^*$ , 218 nm for the  $n \rightarrow \pi^*$ ). CD spectra, therefore, contain detailed information about dissymmetric characteristics of the peptide backbone, the challenge resides in the extraction of this information. An excellent way to improve the CD signal-to-noise ratio, and therefore observe even small differences in these aggregates, is to employ synchrotron radiation as the source of UV light. Here, we use the highly collimated micro-beam light with high photon flux, available at Diamond B23 beamline for SRCD, since it is possible to focus such a beam to a spot area down to 45  $\mu\text{m} \times 15 \mu\text{m}$ , using an objective lens, onto the microfluidic channels. Besides, the SRCD spectra can be measured at different positions along the microfluidic channels using a motorized XY-stage.

### Fabrication of the devices

Due to the strong absorption of many materials in the far-UV range, the fabrication of microfluidic devices for SRCD measurements has, to-date, been limited to fused silica devices

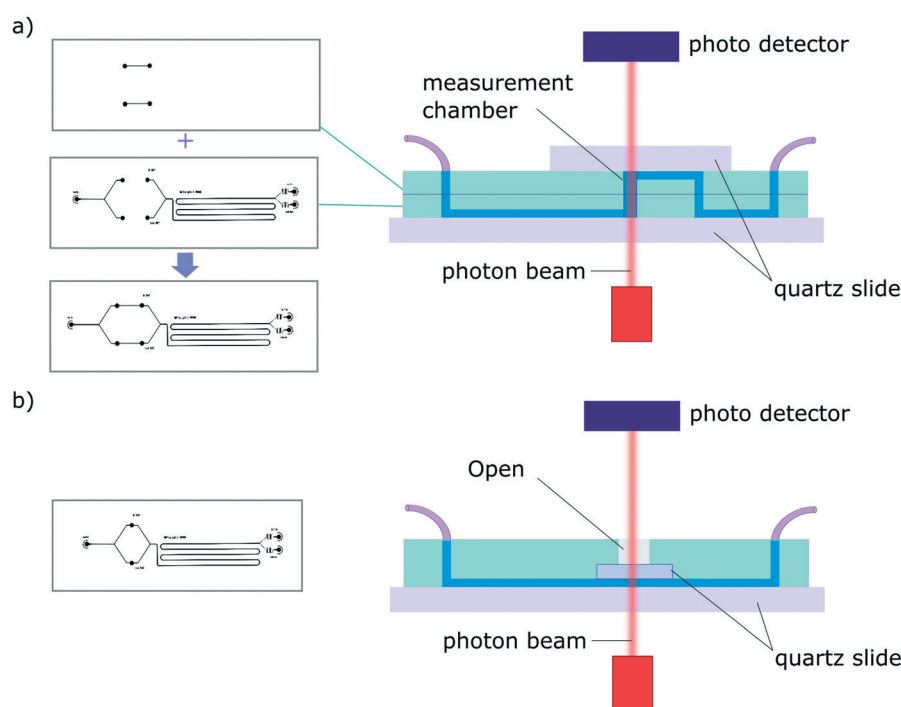


**Fig. 2** Schematic of a typical diffusion devices for the 2 architectures presented. In each case the measurement chambers are confined between quartz windows. The masters are represented on the left and the cross-section of the resulting device is shown on the right (a) architecture 1 consists in two-layer devices. The height of the measurement chamber (equivalent to the path length,  $l$ ) can be tuned by adapting the height of each PDMS layer. (b) Architecture 2 is based on one-master, one-layer devices. The path length,  $l$ , is defined by the height of the channels.

that can only be fabricated in specialised laboratories<sup>35</sup> (see Fig. S1† for a SRCD graph obtained using a conventional PDMS device). We have overcome this problem by developing 2 new microfluidic devices architectures fabricated using conventional PDMS-based soft-lithography, one of the most widely used fabrication technique for microfluidic devices. We have achieved this by integrating, within the microfluidic devices, measurement chambers confined between 2 quartz slides. In order to accommodate for measurement in a wide range of concentrations,  $C$ , we have developed 2 device architectures enabling the tuning of the path length,  $l$  so that the absorption,  $A$ , as defined the Beer–Lambert law:  $A = \epsilon l C$ , where  $\epsilon$  is the molar extinction coefficient, stays between 0.4–1.4, ideally 0.8. Typically, for a 100  $\mu\text{m}$  path length, the protein concentration should be between 0.4–0.8  $\text{mg ml}^{-1}$ .

The first architecture consists of a two-layer device that comprise, at appropriate positions along the microfluidic circuit, measurement chambers confined vertically between two quartz slide windows (Fig. 2a). The fabrication process consists in aligning the 2 complementary PDMS devices, with channels facing out, before plasma bonding. The connections between the 2 layers and to the inlet and outlet ports are made using a biopsy punch. Finally, quartz windows are plasma bonded on each side of the device to seal the channels. The second set of devices is fabricated using a single layer architecture and a one-mould process (Fig. 2b). The fabrication steps consist in pouring uncured PDMS in the master mold and pressing a  $5 \times 5$  mm quartz window (cut from a quartz slide using a diamond scribe) onto the measurement chamber area. Once the device is cured, the structured PDMS is peeled gently, making sure the quartz window stays in place, and the ports are punched. Finally, a quartz slide is plasma bonded onto the device to seal the channels (see Fig. S4†). The second architecture was also tested successfully using a 3D printed master (see Fig. S5.a†).

### Calculation of the diffusion profile

We consider particles diffusing in a fully developed flow in a rectangular microfluidic channel, so the problem can be simplified by time independence and a translationally invariant flow in the channel direction ( $x$  axis). The flow in such a channel is given by the Poiseuille flow. From the incompressible Navier–Stokes equation:

$$\rho[\partial_t v + (v \cdot \nabla)v] = -\nabla p + \eta \nabla^2 v + \rho g \quad (1)$$

we apply time invariance ( $\partial_t v = 0$ ) and translational invariance ( $(v \cdot \nabla)v = 0$ ) to get:

$$\eta[\partial_y^2 + \partial_z^2]v_x(y, z) = \partial_x p(x) \quad (2)$$

This equation can be solved analytically. The following formulation of the solution is symmetrical and converges quickly:<sup>39</sup>

$$v_x(y, z) \propto \sum_{n_y, \text{ odd}} \sum_{n_z, \text{ odd}} \frac{1}{n_y n_z \left( \frac{n_y^2}{W_y^2} + \frac{n_z^2}{W_z^2} \right)} \sin\left(\frac{n_y \pi}{W_y} y\right) \sin\left(\frac{n_z \pi}{W_z} z\right) \quad (3)$$

with  $v_x$  the Poiseuille flow, and  $W_y$  and  $W_z$  the dimensions of the channel in the  $y$  and  $z$  directions.

The general convection–diffusion equation for the local concentration  $c(x, y, z)$  and diffusion coefficient  $D$  is given by:

$$\frac{\partial c}{\partial t} = \nabla \cdot (D \nabla c) - \nabla \cdot (vc) \quad (4)$$

It is similarly simplified by translational invariance of the flow and time invariance:

$$\partial_x c = \frac{D}{v_x} \nabla^2 c \quad (5)$$

Assuming that diffusion in the  $x$  direction is negligible ( $D \partial_x^2 c \ll v_x \partial_x c$ ):

$$\partial_x c = \frac{D}{v_x} (\partial_y^2 + \partial_z^2) c \quad (6)$$

This equation is numerically integrated with a trapezoid method and Neumann boundary conditions. The space step  $dx$  is chosen with the Courant–Friedrichs–Lewy condition:

$$dx = \frac{1}{2D} \min(\delta y, \delta z)^2 \min(v_x) \quad (7)$$

This choice of  $dx$  means the step matrix  $S$  is independent on  $D$  and  $Q$ , the flow rate, given by  $Q = \int dy \int dz v_x(y, z)$ . Defining the dimensionless step size  $dx' = dx \times D/Q$ , the number of steps to reach a position  $L$  is found to be:

$$N_{\text{steps}} = \frac{LD}{dx'Q} \quad (8)$$

The evolution of an initial concentration distribution  $c_0$  can therefore be quickly calculated by repeated matrix squaring. Indeed using  $S_i = S^{2^i}$ , only at most  $\log_2(N_{\text{steps}})$  matrix multiplications are necessary. For example 50 is 110 010 in binary, so  $c_{50} = S_6 \cdot (S_5 \cdot (S_1 \cdot c_0))$ . Fig. S6† shows concentration profiles obtained using the above for insulin monomers.

## 3 Results and discussions

### 3.1 Validation using simple solutions

In order to validate the compatibility of the two device architectures with SRCD, we have proceeded to a range of experiments using model protein systems. BSA monomers and

insulin monomers and amyloid fibrils formed from the same proteins<sup>40,41</sup> were tested in a range of microfluidic devices under flow and static conditions and compared with the spectra obtained in static mode in dedicated flow cells, using both SRCD and a bench top CD spectropolarimeter Chirascan Plus.

In the first set of separation experiments, solutions of insulin monomers ( $0.2 \text{ mg ml}^{-1}$ ) or fibres ( $0.4 \text{ mg ml}^{-1}$ ) were injected alongside a buffer solution (water) and SRCD spectra were measured in the two measurement chambers, each collecting 50% of the solution, after a diffusion length of 90  $\mu\text{m}$  (Fig. 3a). The high diffusion chamber collects a fraction of the small, high diffusion coefficient molecules, while the low diffusion measurement chambers retains most of the larger molecules, with a lower diffusion coefficient (Fig. 3a and b). The flow rates were 30 and  $300 \mu\text{l h}^{-1}$  for the insulin and the buffer solutions respectively. The devices were made using the first architecture and the heights of the measurement chambers, corresponding to the path length, ranged typically between 3 and 5 mm. The spectra obtained for the monomers, with a typical high  $\alpha$ -helical content (see Fig. 3c), and fibres, with a stronger  $\beta$ -sheet signal (see Fig. S7<sup>†</sup>), are in good agreement with the results obtained using benchtop CD instrument in static mode and confirm that neither the devices, nor the flow rate, induce any artefact (see Fig. S8<sup>†</sup> for the spectra and secondary structure of undiluted solutions using a benchtop CD instrument).

In order to verify the efficiency of the diffusion-based separation, we have measured the concentration of each fraction and compared it with the expected theoretical value. The concentration ratios were measured by dividing the amplitude of the CD signal at 208 nm (monomer) and 222 nm (fibre) in each chamber by the corresponding amplitude of the total concentration. These values were compared to the concentration expected due to diffusion, as calculated using the area under the theoretical concentration profile (Fig. 3b). The measured and expected (calculated) fraction in each chamber show excellent agreement as detailed in Table 1.

We also measured the concentration profile of a solution of insulin monomers ( $2 \text{ mg ml}^{-1}$ ) across a 2000  $\mu\text{m}$  wide

**Table 1** Comparison between expected (calculated) and measured fraction of insulin monomer and fibres in each chamber. A reference value of 208 nm was chosen for the monomers as it corresponds to the  $\pi \rightarrow \pi^*$  excitonic transition of  $\alpha$ -helices; 222 nm is representative of the  $n \rightarrow \pi^*$  of  $\beta$ -sheet rich compounds such as insulin fibres

	Measured	Calculated
Amyloid fibrils (222 nm)	2.3%	1.1%
Monomers (208 nm)	13.8%	11.7%

microfluidic channel, using the second architecture with a 50  $\mu\text{m}$  high channel, and flow rates of 30 and  $300 \mu\text{l h}^{-1}$  for the monomers and buffer solution respectively. The SRCD signal amplitude at 208 nm was measured continuously for 1 minute in 5 positions across the channel width. The normalised average amplitude points (and standard deviation) show a good match with the expected concentration profile as shown in Fig. 4.

Finally, we performed a time-dependent dilution experiment, using BSA ( $0.2 \text{ mg ml}^{-1}$ ,  $60 \mu\text{l h}^{-1}$ ) in a Y-junction channel fabricated with a 3D printed master mould based on the second architecture. The measurement, limited by the time needed to acquire a full spectrum, is performed at the end of the channel, across its entire width, where the original sample gets diluted due to the progressive introduction of the aqueous buffer solution from  $0 \mu\text{l h}^{-1}$  to  $60 \mu\text{l h}^{-1}$ . The spectra shown in Fig. 5 do not exhibit any distortions, as confirmed after normalisation (Fig. S5.b<sup>†</sup>). For faster experiments, continuous measurement at a single wavelength can be performed.

The validation results presented above, obtained using simple protein solutions, constitute a proof that the different microfluidics device architectures proposed are compatible with SRCD.

### 3.2 Resolution in complex mixtures

Finally, we explore the possibility to resolve complex protein mixtures using the methods and devices detailed earlier. To

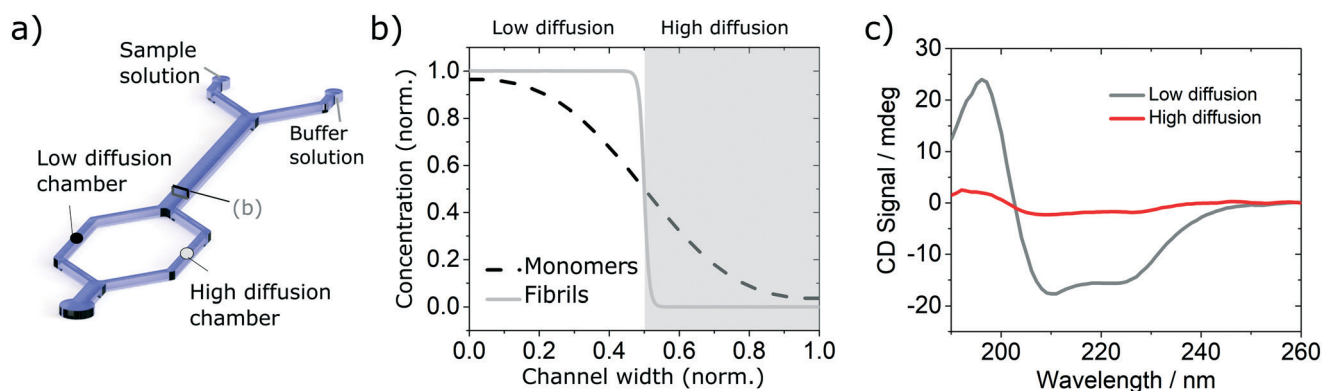


**Fig. 3** Validation of the diffusion based separation using simple solutions of insulin monomers. (a) Simplified sketch of the device used with indication of the low (black circle) and high (grey circle) diffusion chambers. (b) Diffusion profile and fractions collected at the end of the diffusion channel. (c) SRCD spectra of insulin monomer in each chamber.

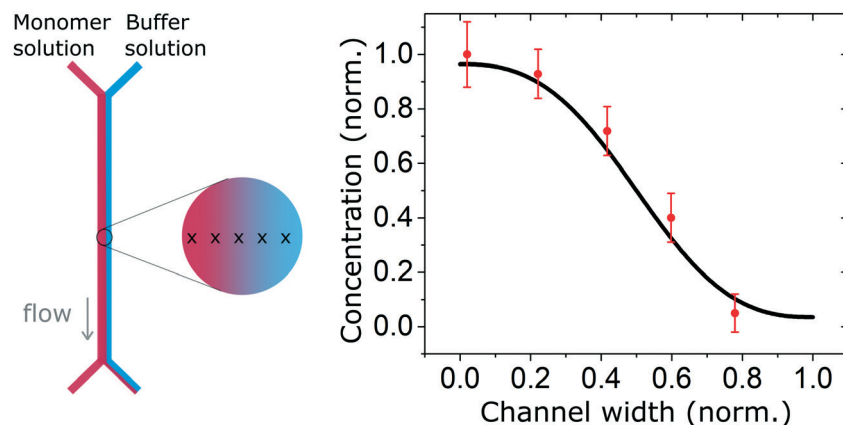


Fig. 4 Concentration profile of a solution of insulin monomers ( $2 \text{ mg ml}^{-1}$ ) across a  $2000 \mu\text{m}$  wide microfluidic channel with flow rates of 30 and  $300 \mu\text{l h}^{-1}$  for the monomers and buffer solution respectively. The high energy photon beam was positioned using the motorised stage in 5 locations across the channel and the SRCD signal amplitude, taken at 208 nm, was measured continuously during one minute and averaged. The measured profile shows a good agreement with the expected (simulated) profile.

this effect, we explored solutions comprised of insulin monomers and fibrils, mixed at different concentrations depending on the devices used. The case of a microfluidic device of  $25 \mu\text{m}$  path length used to resolve a 1:1 mixture of monomers ( $3 \text{ mg ml}^{-1}$ ) and fibrils ( $1 \text{ mg ml}^{-1}$ ) is shown in Fig. 6. By analysing the spectrum of the mixture and calculating the secondary structures, it is not possible to resolve the different fractions that compose it, without an *a priori* knowledge of the individual fractions. However, if one can isolate a single constituent it then becomes possible to resolve the mixture. The case of a 2 component mixture is straight forward and is demonstrated experimentally in this manuscript (Fig. 6). The case of more complex mixtures is discussed later.

Using the H-filter microfluidic separation device architecture presented herein, we isolate a fraction of monomers from the mixture. Using an 18 cm long diffusion channel,

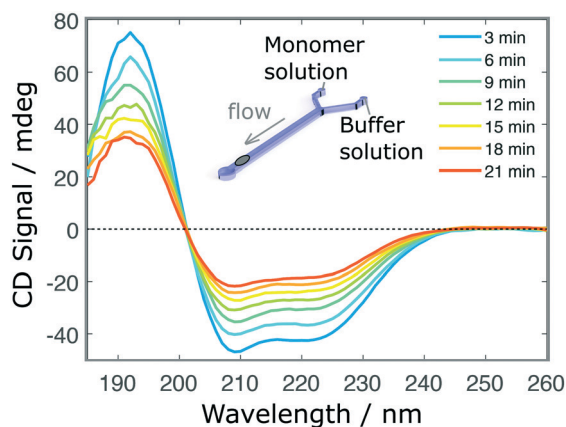
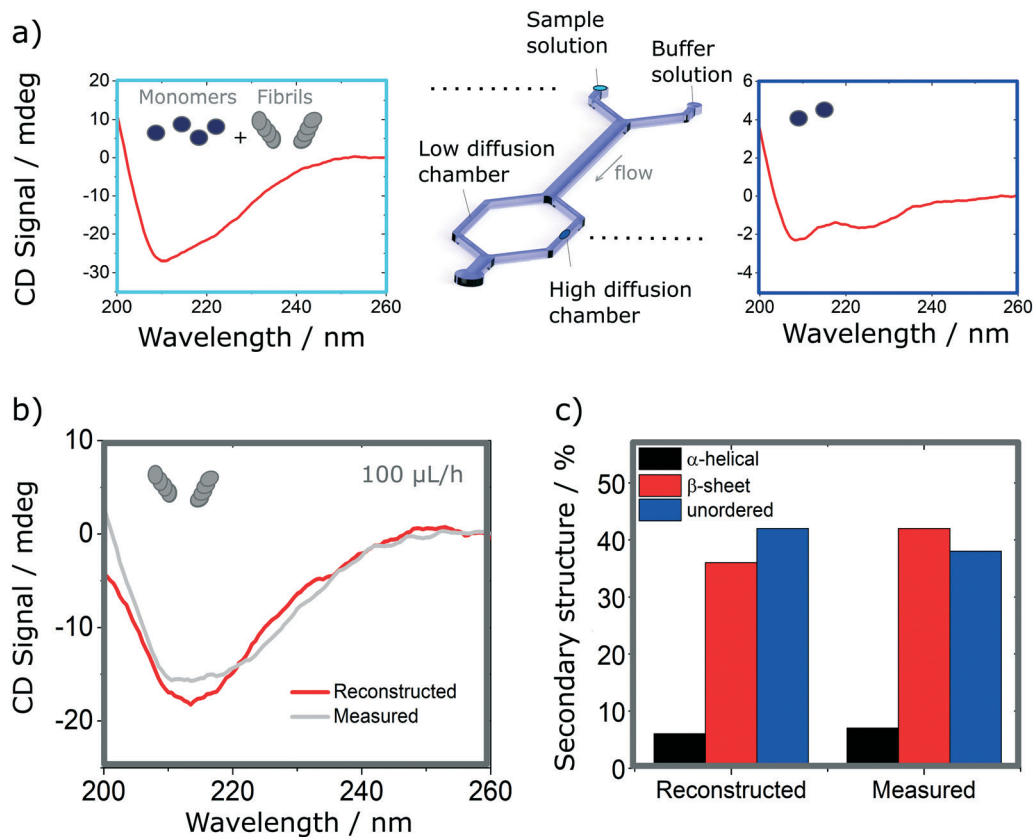


Fig. 5 Time-dependent measurements. SRCD spectra of BSA protein (initial concentration  $0.3 \text{ mg ml}^{-1}$ ) in a dilution experiment as a function of time. In this case, the channel is initially loaded with the sample solution and the buffer is introduced progressively at  $30 \mu\text{l h}^{-1}$  in a Y-junction microfluidic device fabricated by soft-lithography using a 3D printed master mould.

one can direct 22% of monomers and no fibres (0%) in the high-diffusion chamber by collecting one third of the flow (see Fig. 6a, right hand-side spectrum). The amplitude of the spectrum collected is then adjusted by a multiplication factor (in this case,  $100/22 = 4.55$ ) to account for the 100% of monomer present in the mixture and subtracted from the spectrum obtained for the mixture. The resulting reconstructed spectrum, shown in Fig. 6b, compares well with the spectrum of a fibril solution (of the same concentration) measured in the same chamber. This observation is confirmed by the analysis of the secondary structure, calculated using BeStSel, a method for the secondary structure determination and fold recognition from protein circular dichroism spectra.<sup>42</sup> Fig. 6c shows that the  $\alpha$ -helical content for the reconstructed and measured spectra are identical (6 and 7% for the reconstructed and measured spectra respectively). The  $\beta$ -sheet and unordered contents, however, show small discrepancies. The  $\beta$ -sheet content is of 36% for the reconstructed and 42% for the measured spectra while the unordered content is of 42 and 38% for the reconstructed and measured spectra respectively. The differences observed can be attributed to small distortions of the spectrum that can arise due to variation of the microfluidics chip position with respect to the photon beam between the measurements, the measurement in dynamic mode and resulting flow fluctuations, as well as the low concentration collected, imposed by the necessity to exclude fibres from the high-diffusion chamber. It is noted also that even though monomers are stable at room temperature and neutral pH, they can start to aggregate with the fibrils, which act as catalysts.<sup>43</sup> However, in this case, such conversion is very slow and, therefore, the content of the solutions studied is expected to be stable for the duration of the experiments presented herein (see Fig. S9† for details).

The approach described above can also be adapted to resolve more complex mixtures. Microfluidic diffusion-based separation enables the exclusion of species above a given



**Fig. 6** Resolution of mixtures of insulin monomer and fibrils using analytical diffusion-based microfluidics separation and SRCD. It is not possible to resolve the mixture from its SRCD spectrum (a, left). However, by isolating the monomers (a, right), it is possible to reconstruct the fibrils spectrum after subtracting the spectrum of the resolved fraction from the that of the total mixture. (b). The spectrum shows good agreement with the measured spectrum in the same conditions (b) as confirmed by the analysis of their secondary structures (c).

hydrodynamic radius, in a single separation step. Even though it would theoretically be possible to isolate the smallest molecule in the complex mixture (*e.g.* a monomer), it has been shown that it is not possible to precisely resolve biomolecules unless their hydrodynamic radii differ by at least a factor three.<sup>44</sup> Therefore, in order to increase the separation resolution, one should combine the approach with other high resolution microfluidic separation techniques, such as free-flow electrophoresis that enables the selection of biomolecules based on their electrophoretic mobility.<sup>45–47</sup> However, ultimately, the detection of a single constituent from a mixture will be limited by the sensitivity of the measurement technique. Nevertheless, the separation of a heterogeneous mixture into less complex, yet well-resolved, fractions is expected to provide further insights into complex biological phenomena.

## 4 Conclusions

The study of heterogeneous mixtures of proteins is challenging yet important for a number of practical applications. Current biophysical methods and devices are usually not well-suited to study, in molecular detail, heterogeneous mixtures in their native environment while retaining the temporal information. In this manuscript, we show that the combination

of microfluidic free-flow separation and label-free bulk measurement techniques such as synchrotron radiation circular dichroism can overcome such issues. In particular, we demonstrate that a diffusional sizing microfluidic device can be used to isolate into a well-resolved fraction, insulin monomers from a heterogeneous mixture of insulin monomers and fibrils. Using the spectrum from this fraction, it is possible to extract information about the missing fraction and finally resolve the entire heterogeneous mixture.

In order to make the results presented in this study available to a broad scientific community, we have developed new fabrication methods to integrate far-UV compatible measurement chambers (confined between quartz windows) into PDMS based microfluidic devices fabricated using conventional soft-lithography approaches. Two device architectures, which enable the measurement of a wide range of concentrations, are presented, characterised and validated using the highly collimated and high photon-flux microbeam light available at Diamond Light Source B23 beamline for SRCD.

The device architecture presented herein can also be used in combination with other sensing modalities requiring far-UV transparency and more generally, the principle can also be adapted to other bulk measurement techniques. In summary, the possibility to precisely separate a heterogeneous mixture into well-resolved, simpler fractions opens up a

range of opportunities for the study of complex biological phenomena. In particular, such developments open up interesting perspective to study protein misfolding and aggregation diseases such as Alzheimer's and Parkinson's diseases and may provide time-resolved information about the protein aggregation pathway.

## Authors contributions

G. S., T. P. J. K. and J. C. conceived the project. C. B., T. K., D. C., I. C. M., P. K. C., T. J., R. H. and J. C. performed the experiments. I. C. M., Y. Z., Q. A. E. P., T. J. and R. H. provided resources. C. B., Q. A. E. P., R. H., G. S. and J. C. analysed the results. M. D., G. S., T. P. J. K. and J. C. supervised the work. C. B. and J. C. wrote the original manuscript. All authors commented on the manuscript.

## Conflicts of interest

There are no conflicts to declare.

## Acknowledgements

The research leading to these results has received funding from the European Research Council under the European Union's Seventh Framework Programme (FP7/2007-2013) through the ERC grant PhysProt (agreement no. 337969, T. P. J. K.). We gratefully acknowledge financial support from the Biotechnology and Biological Sciences Research Council (agreement no. BB/J002119/1), the Wellcome Trust, the Frances and Augustus Newman Foundation, the Lundbeck Foundation (C. B.), the Nanotechnologies Doctoral Training Centre in Cambridge (NanoDTC Cambridge EP/L015978/1, T. K.), the Institutional Links grant, ID 352360246, under the Newton-Katip Celebi Fund partnership (J. C.), the European Union's Horizon 2020 research and innovation programme under grant agreement no. 674979-NANOTRANS (Q. A. E. P.), the MSCA-IF grant 660351-EmuCam (D. C.), and CONACYT and Cambridge Trust (I. C. M.).

## Notes and references

- 1 T. P. J. Knowles, M. Vendruscolo and C. M. Dobson, *Nat. Rev. Mol. Cell Biol.*, 2014, **15**, 384–396.
- 2 N. J. Greenfield, *Nat. Protoc.*, 2006, **1**, 2876–2890.
- 3 S. Brahm and J. Brahm, *J. Mol. Biol.*, 1980, **138**, 149–178.
- 4 W. K. Surewicz, H. H. Mantsch and D. Chapman, *Biochemistry*, 1993, **32**, 389–394.
- 5 J. Seo, W. Hoffmann, S. Warnke, X. Huang, S. Gewinner, W. Schöllkopf, M. T. Bowers, G. von Helden and K. Pagel, *Nat. Chem.*, 2017, **9**, 39–44.
- 6 A. E. Smith, Z. Zhang, G. J. Pielak and C. Li, *Curr. Opin. Struct. Biol.*, 2015, **30**, 7–16.
- 7 K. Wuthrich, *Science*, 1989, **243**, 45–50.
- 8 G. Meisl, X. Yang, E. Hellstrand, B. Frohm, J. B. Kirkegaard, S. I. a. Cohen, C. M. Dobson, S. Linse and T. P. J. Knowles, *Proc. Natl. Acad. Sci. U. S. A.*, 2014, **111**, 9384–9389.
- 9 M. H. Horrocks, S. F. Lee, S. Gandhi, N. K. Magdalinou, S. W. Chen, M. J. Devine, L. Tosatto, M. Kjaergaard, J. S. Beckwith, H. Zetterberg, M. Iljina, N. Cremades, C. M. Dobson, N. W. Wood and D. Klenerman, *ACS Chem. Neurosci.*, 2016, **7**, 399–406.
- 10 M. Pfammatter, M. Andreasen, G. Meisl, C. G. Taylor, J. Adamcik, S. Bolisetty, A. Sánchez-Ferrer, D. Klenerman, C. M. Dobson, R. Mezzenga, T. P. J. Knowles, A. Aguzzi and S. Hornemann, *Anal. Chem.*, 2017, **89**, 12306–12313.
- 11 M. R. H. Krebs, E. H. C. Bromley and A. M. Donald, *J. Struct. Biol.*, 2005, **149**, 30–37.
- 12 J. Adamcik, J.-M. Jung, J. Flakowski, P. De Los Rios, G. Dietler and R. Mezzenga, *Nat. Nanotechnol.*, 2010, **5**, 423–428.
- 13 A. F. Oberhauser, P. E. Marszalek, M. Carrion-Vazquez and J. M. Fernandez, *Nat. Struct. Mol. Biol.*, 1999, **6**, 1025–1028.
- 14 A. W. P. Fitzpatrick, B. Falcon, S. He, A. G. Murzin, G. Murshudov, H. J. Garringer, R. A. Crowther, B. Ghetti, M. Goedert and S. H. W. Scheres, *Nature*, 2017, **547**, 185–190.
- 15 M. Bucciattini, E. Giannoni, F. Chiti, F. Baroni, L. Formigli, J. Zurdo, N. Taddei, G. Ramponi, C. M. Dobson and M. Stefani, *Nature*, 2002, **416**, 507–511.
- 16 F. S. Ruggeri, G. Longo, S. Faggiano, E. Lipiec, a. Pastore and G. Dietler, *Nat. Commun.*, 2015, **6**, 7831.
- 17 D. Pinotsi, C. H. Michel, A. K. Buell, R. F. Laine, P. Mahou, C. M. Dobson, C. F. Kaminski, G. S. Kaminski Schierle and G. S. K. Schierle, *Proc. Natl. Acad. Sci. U. S. A.*, 2016, **113**, 3815–3819.
- 18 M. H. Horrocks, L. Rajah, P. Jönsson, M. Kjaergaard, M. Vendruscolo, T. P. J. Knowles and D. Klenerman, *Anal. Chem.*, 2013, **85**, 6855–6859.
- 19 F. S. Ruggeri, J. Habchi, A. Cerreta and G. Dietler, *Curr. Pharm. Des.*, 2016, **22**, 3950–3970.
- 20 A. T. Petkova, R. D. Leapman, Z. Guo, W.-M. Yau, M. P. Mattson and R. Tycko, *Science*, 2005, **307**, 262–265.
- 21 D. Pinotsi, A. K. Buell, C. M. Dobson, G. S. Kaminski Schierle and C. F. Kaminski, *ChemBioChem*, 2013, **14**, 846–850.
- 22 G. W. Somsen, W. Morden and I. D. Wilson, *J. Chromatogr. A*, 1995, **703**, 613–665.
- 23 F. J. Moy, K. Haraki, D. Mobilio, G. Walker, R. Powers, K. Tabei, H. Tong and M. M. Siegel, *Anal. Chem.*, 2001, **73**, 571–581.
- 24 H. Liu, S. J. Berger, A. B. Chakraborty, R. S. Plumb and S. A. Cohen, *J. Chromatogr., B*, 2002, **782**, 267–289.
- 25 M. Elizabeth, M. Ahmed and M. Nick, *J. Synchrotron Radiat.*, 2004, **11**, 314–318.
- 26 P. G. Righetti, N. Camprostrini, J. Pascali, M. Hamdan and H. Astner, *Eur. J. Mass Spectrom.*, 2004, **10**, 335–348.
- 27 J. F. Carpenter, T. W. Randolph, W. Jiskoot, D. J. A. Crommelin, C. R. Middaugh and G. Winter, *J. Pharm. Sci.*, 2010, **99**, 2200–2208.
- 28 T. Arakawa, D. Ejima, T. Li and J. S. Philo, *J. Pharm. Sci.*, 2010, **99**, 1674–1692.
- 29 J. Charmet, P. Arosio and T. P. J. Knowles, *J. Mol. Biol.*, 2018, **430**, 565–580.

- 30 T. A. Duncombe, A. M. Tentori and A. E. Herr, *Nat. Rev. Mol. Cell Biol.*, 2015, **16**, 554–567.
- 31 T. P. J. Knowles, D. A. White, A. R. Abate, J. J. Agresti, S. I. A. Cohen, R. A. Sperling, E. J. De Genst, C. M. Dobson, D. A. Weitz, E. J. D. Genst, C. M. Dobson and D. A. Weitz, *Proc. Natl. Acad. Sci. U. S. A.*, 2011, **108**, 14746–14751.
- 32 J. J. Agresti, E. Antipov, A. R. Abate, K. Ahn, A. C. Rowat, J.-C. Baret, M. Marquez, A. M. Klibanov, A. D. Griffiths and D. A. Weitz, *Proc. Natl. Acad. Sci. U. S. A.*, 2010, **107**, 4004–4009.
- 33 J. P. Brody and P. Yager, *Sens. Actuators, A*, 1997, **58**, 13–18.
- 34 R. Hussain, T. Javorfi and G. Siligardi, *J. Synchrotron Radiat.*, 2012, **19**, 132–135.
- 35 A. S. Kane, A. Hoffmann, P. Baumgärtel, R. Seckler, G. Reichardt, D. A. Horsley, B. Schuler, O. Bakajin, P. Baumga, R. Seckler, G. Reichardt, D. A. Horsley, B. Schuler and O. Bakajin, *Anal. Chem.*, 2008, **80**, 9534–9541.
- 36 P. K. Challa, T. Kartanas, J. Charmet and T. P. J. Knowles, *Biomicrofluidics*, 2017, **11**, 014113.
- 37 Y. Xia and G. Whitesides, *Annu. Rev. Mater. Sci.*, 1998, **28**, 153–184.
- 38 G. Silligardi and R. Hussain, *Structural Proteomics*, Springer New York, New York, NY, 2015, vol. 1261.
- 39 M. Spiga and G. L. Morino, *Int. Commun. Heat Mass Transfer*, 1994, **21**, 469–475.
- 40 J. L. Jiménez, E. J. Nettleton, M. Bouchard, C. V. Robinson, C. M. Dobson and H. R. Saibil, *Proc. Natl. Acad. Sci. U. S. A.*, 2002, **99**, 9196–9201.
- 41 M. I. Ivanova, S. A. Sievers, M. R. Sawaya, J. S. Wall and D. Eisenberg, *Proc. Natl. Acad. Sci. U. S. A.*, 2009, **106**, 18990–18995.
- 42 A. Micsonai, F. Wien, L. Kernya, Y.-H. Lee, Y. Goto, M. Refregiers and J. Kardos, *Proc. Natl. Acad. Sci. U. S. A.*, 2015, **112**, E3095–E3103.
- 43 S. I. a. Cohen, M. Vendruscolo, C. M. Dobson and T. P. J. Knowles, *J. Mol. Biol.*, 2012, **421**, 160–171.
- 44 P. Arosio, T. Muller, L. Rajah, E. V. Yates, F. A. Aprile, Y. Zhang, S. I. A. Cohen, D. A. White, T. W. Herling, E. J. De Genst, S. Linse, M. Vendruscolo, C. M. Dobson and T. P. J. Knowles, *ACS Nano*, 2016, **10**, 333–341.
- 45 T. W. Herling, P. Arosio, T. Müller, S. Linse and T. P. J. Knowles, *Phys. Chem. Chem. Phys.*, 2015, **17**, 12161–12167.
- 46 B. R. Fonslow and M. T. Bowser, *Anal. Chem.*, 2006, **78**, 8236–8244.
- 47 M. Shao, X. Xing and C.-C. Liu, *Electroanalysis*, 1994, **6**, 245–249.